High-resolution low-energy electron-diffraction analysis of the Pb(110) roughening transition

H.-N. Yang, T.-M. Lu, and G.-C. Wang
Department of Physics, Rensselaer Polytechnic Institute, Troy, New York 12180-3590
(Received 20 August 1990)

We present a detailed line-shape analysis of the high-resolution low-energy electron-diffraction angular profiles measured from the Pb(110) surface undergoing a roughening transition. Experimentally, we show that the effects of multiple scattering and the thermal diffuse scattering do not make significant contributions to the line shape and therefore do not affect the structural information extracted from the angular intensity distribution of the diffracted beams associated with a surface undergoing the roughening transition. We have measured the effect of anisotropy in the roughening of a low-index plane metal surface. For the Pb(110) surface, the ratio of anisotropic interaction energies is estimated from the measurement to be $J_x:J_y=3.46:1$. In addition, we have also measured an enhanced surface anharmonicity starting around 380 K, which is closely related to the anomalous derelaxation of the top layers previously observed by the high-energy ion-channeling technique. This derelaxation may be the major cause for the roughening transition occurring in the Pb(110) surface.

I. INTRODUCTION

Recently there has been very active research in the study of thermal roughening phase transitions in low-index metal surfaces. Examples are Ag,[1] Cu,[2] Ni,[3] and Pb (Ref. 4) surfaces. At least two of these surfaces[1,4] appear to exhibit the conventional Kosterlitz-Thouless type[5] of infinite order transition. We have presented a brief report on the observation of such a roughening transition in the Pb (110) surface using the high-resolution low-energy electron-diffraction (HRLEED) technique.[4] In this paper we report a detailed line-shape analysis of the HRLEED angular profiles obtained from the Pb (110) surface undergoing a roughening transition. We show experimentally that the effects of multiple scatterings and the thermal diffuse scattering do not make significant contributions to the line shape and therefore do not affect extraction of the structural information of the surface undergoing the roughening transition from the angular intensity distribution of the HRLEED beams. We have measured the effect of anisotropy in the roughening of a low-index plane metal surface which has been predicted and discussed quite extensively in the last few years.[6]

II. HRLEED EXPERIMENT RESULTS

The basic experimental arrangement has been described previously.[4,7] The very fine resolution of the HRLEED beam angular profile, which has a width less than 0.006 Å^{-1}, allows us to detect not only a slight change of the peak width but also the tail shape of a beam profile very accurately. The x-ray Laue picture and later HRLEED data on the Pb(110) surface indicate that its misorientation and the mosaic angle are less than 0.1°. In order to reduce the step density in the surface one needs to choose an appropriate annealing temperature. By testing the range of annealing temperature from 300 to 590 K, we find that ~360 K is the most effective annealing temperature to eliminate the steps. This annealing temperatures gives the narrowest diffraction beams as determined by the full width at half maximum (FWHM) of the angular profile obtained using the HRLEED. The major experimental results are given as follows.

A. Surface perfection and local defects

We have measured the angular profiles of the (00), (10), and (01) beams as a function of the incident electron beam energy E. In the HRLEED system, since the outgoing beam with wave vector $\mathbf{k}_0$ is diffracted at a constant angle, ~7.5°, with respect to the incident beam of a wave vector $\mathbf{k}_i$,[7,8] the relation between E and the total momentum transfer $\mathbf{S}$, under the elastic scattering condition, can be expressed as

$$|\mathbf{S}|=|\mathbf{k}_o-\mathbf{k}_i|=2|\mathbf{k}_i|\cos(7.5°/2)$$
$$=4\pi\cos(3.75°)\sqrt{E/150.4}\ . \quad (1)$$

The fcc (110) surface has an ABAB stacking structure, as shown in Figs. 1(a) and 1(b). The phase difference φ of electrons scattered from neighboring terraces separated by a monoatomic step, can be written as[9]

$$\varphi=\begin{cases} S_\perp t & \text{for the (00) beam} \\ S_\perp t\pm\pi & \text{for the (10) or (01) beam}\ , \end{cases} \quad (2)$$

with

$$S_\perp=\begin{cases} |\mathbf{S}| & \text{for the (00) beam} \\ [|\mathbf{S}|^2-(2\pi/a)^2]^{1/2} & \text{for the (01) beam} \\ [|\mathbf{S}|^2-(2\pi/b)^2]^{1/2} & \text{for the (10) beam}\ , \end{cases} \quad (3)$$

where $S_\perp$ is the momentum transfer perpendicular to the

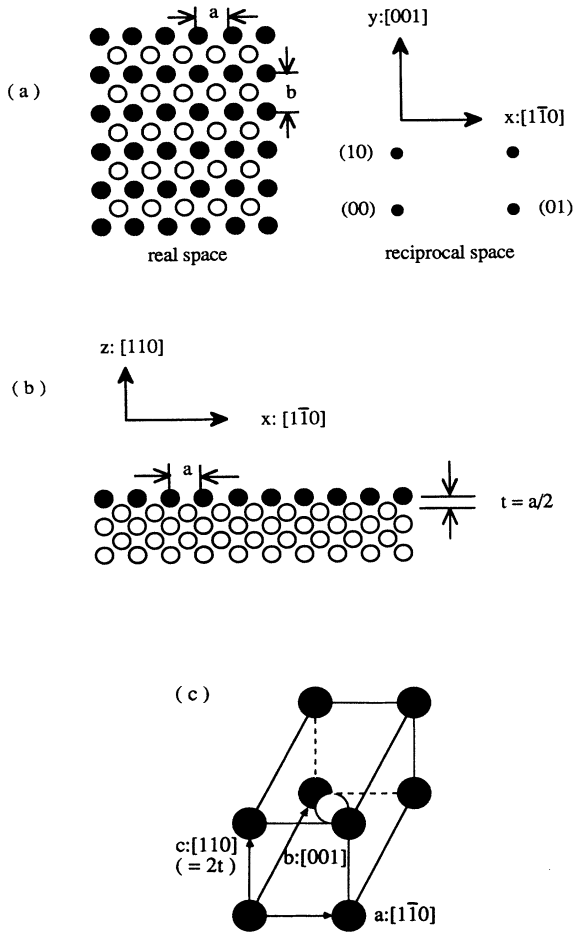

FIG. 1. The fcc(110) surface structure. (a) Top view of the real space surface structure and the corresponding reciprocal space structure. The solid circles represent the first layer atoms and the open circles represent the second layer atoms. (b) Side view of the surface structure. (c) The fcc(110) surface expressed in the body-centered tetragonal unit cell. The first layer atoms are represented by the solid circles in the top face of this tetragonal unit cell and the atoms in the third layer are also solid circles but located in the bottom face. One of the second layer atoms is shown in the center as the open circle.

surface. As defined in Figs. 1(a) and 1(b), t is the step height along the surface normal and a and b are the lengths of the unit vectors along the $[1\bar{1}0]$ and [001] directions, respectively. The definitions of the (01) and (10) beams are also given in Fig. 1(a). $\varphi=2m\pi$ corresponds to the in-phase (constructive) diffraction conditions and $\varphi=(2m+1)\pi$ corresponds to the out-of-phase (destructive) diffraction conditions, where $m=0,\pm1,\pm2,\ldots$. Since no in-plane reconstruction has been observed, it is reasonable to use the bulk lattice constants $a=3.50$ Å and $b=\sqrt{2}a=4.95$ Å as the lengths of the unit mesh vectors. The lengths a and b agree well with our experimental a and b obtained by measuring the magnitudes of the reciprocal unit mesh vectors: $G_{01}=2\pi/a$ and $G_{10}=2\pi/b$.

In Fig. 2, shown as the solid dots, we plot the measured FWHM's of the (00), (10), and (01) beam profiles at room temperature as a function of $S_\perp t$ determined by Eqs. (1) and (3) which relate $S_\perp$ to the measured electron energy E. The step height t is chosen to be the bulk value, i.e., $t=1.75$ Å. As we shall see later, within the experimental uncertainty (±0.05 Å), it is consistent with the measured oscillation period of the FWHM's in the high-temperature region where the surface steps are induced. The period of the oscillation is a measure of the step height.[9] Although there exists an inward relaxation on the top layer at $T\leq 380$ K,[10–12] the experimental determination of t using the oscillation period is almost impossible in this low-temperature region where no oscillation behavior could be observed. In addition, the angular profiles of the (00) beam at room temperature, for both the in-phase and out-of-phase conditions, are plotted in Fig. 3.

At room temperature, the peak width and the angular profile at the out-of-phase condition are practically the same as those at the in-phase condition, as seen in Figs. 2 and 3. There is no oscillatory behavior in FWHM's at room temperature. All the profiles are smooth and have no shoulder structure or peak splitting. These facts indicate that the surface is practically flat. The resolving power of our HRLEED is better than 2000 Å,[13] but the FWHM at the in-phase condition for this Pb(110) surface is about 0.02 Å^{-1}. The additional broadening is basically due to the mosaic angles between micrograins.[8] Treating the FWHM at the in-phase condition as an effective instrument response width (which is 0.019±0.002 Å^{-1} in the [001] azimuth and is 0.014±0.002 Å^{-1} in the $[1\bar{1}0]$ azimuth), we estimate that the ordered surface domains are at least 700 Å.[4]

There is a slight difference in the profiles between the in-phase and out-of-phase conditions: a broad diffuse background can be detected at the out-of-phase condition, but not at the in-phase condition, as seen in Fig. 3. The existence of a background intensity is usually due to the surface imperfections, e.g., local steps, point defects such as vacancies and adatoms, high angle mosaic structures, and inelastic phonon scattering. We can immediately rule out the possibility of a high angle mosaic structure and inelastic phonon scattering. This is because these two types of defects would give a similar diffuse scattering at both the in-phase and out-of-phase conditions, which is not consistent with our data. We can also rule out the vacancy or adatom effects, since these defect structures would give a uniform background[14] instead of the broad diffuse intensity localized in the vicinity of Bragg diffraction peaks. Comparing the line shape at the out-of-phase condition with that at the in-phase condition, we conclude that only local steps can give such a broad background. At the in-phase condition there is no detectable diffuse background and its profile can be fitted very well with a single Gaussian function corresponding to the instrument response. An analysis of the angular profile at the out-of-phase condition shows that the diffuse background can be fitted very well by a broad Lorentzian function. The peak intensity of this Lorentzi-

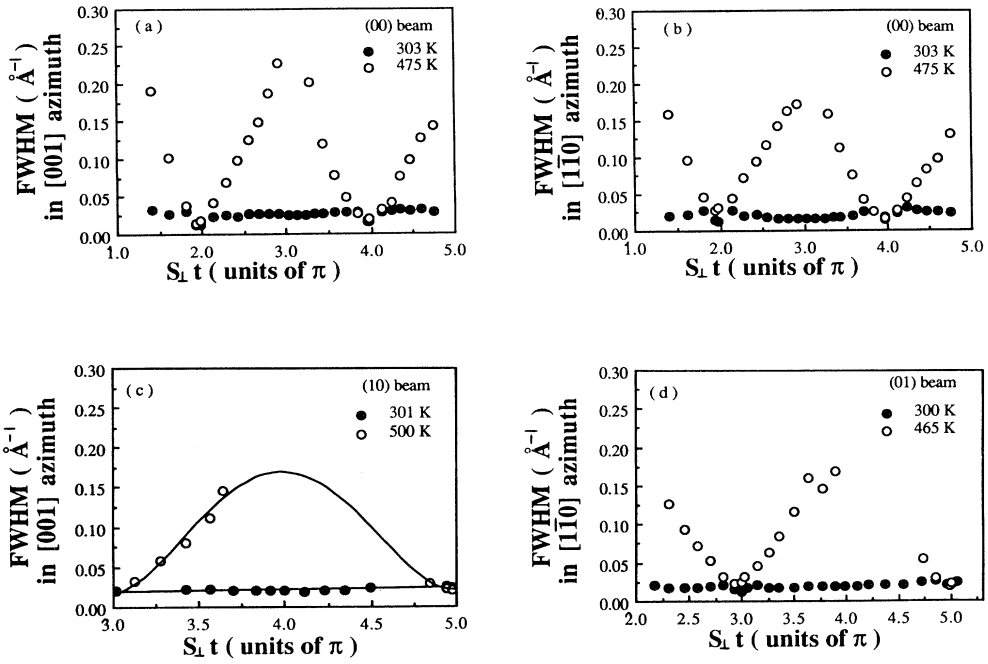

FIG. 2. The FWHM's of the (00), (01), and (10) diffracted beams as a function of $S_\perp t$ at $T\sim 300$ K and $T\sim 480$ K, where $S_\perp$ is the momentum transfer perpendicular to the Pb(110) surface and t ($=1.75$ Å) is the single step height. The oscillation behaviors of the (01) and (10) beams have a phase shift of π relative to that of the (00) beam.

an component is about 15% of the total peak intensity at exactly the Bragg condition. As will be discussed in Sec. IV, these steps exhibit a short-range behavior and are localized both laterally and vertically which can be called "local steps." A possible mechanism for the generation of these local steps on a flat surface is the preroughening effect predicted by Rommelse and den Nijs recently.[15]

Thus we conclude that the room-temperature Pb(110) surface is considered to be very flat and contains very few defects.

B. Temperature-dependent angular profiles

As the temperature is raised above room temperature, the FWHM's for the (00), (10), and (01) beams at the out-of-phase conditions increase drastically above 400 K. In Fig. 4, the FWHM of the (00) beam at the out-of-phase condition is plotted as a function of temperature [the (10) and (01) beams have similar behaviors]. In Fig. 2, we also plot the FWHM as a function of $S_\perp t$ at high temperatures ~ 480 K in comparison with its behavior at the room temperature. At high temperatures, the FWHM's for both the specular beam and the higher-order beams change dramatically from constant values to the oscillatory behavior, which indicates the proliferation of the atomic steps on the surface. Figure 2 also shows that the oscillation of the FWHM's of the (01) and (10) beams has a π phase difference from that of the (00) beam, which is consistent with Eq. (2) and is basically due to the ABAB stacking structure. The average terrace width can be obtained from the amplitude of the oscillation.[9] It is estimated from the (00) beam that the terrace width is ~ 300 Å at 428 K and ~ 35 Å at 475 K. This is a direct indication of the increasing step density which is related to the roughening of the Pb(110) surface.

The angular profile not only undergoes a dramatic broadening, but also develops a substantial tail at ~ 410 K. In Fig. 5, we display the evolution of the angular profiles of the (00) beam along both the [001] and [1$\bar{1}$0] azimuths at different temperatures with $E=27.0$ eV, which corresponds to an out-of phase of 3π.

The observed broadening of the profiles as well as the increase of the intensity in the tails at the out-of-phase diffraction condition are a result of the creation of high density steps in the surface. In principle, multiple scatterings and thermal diffuse scattering may contribute to the change of the profile shape. These effects, if they are significant, might obscure the interpretation of the data and are always of concern in low-energy electron diffraction. Theoretical calculation and prediction of these effects on the profile shape have been very difficult. In our opinion, a reliable conclusion about these effects on the profile shape can only come from the experiment. If these effects were important and if they gave significant contributions to the observed change of the profile shape at the out-of-phase diffraction condition, they should give a similar change of the profile shape at the in-phase diffraction condition at the same temperature. Experimentally we found that that is not the case. In Fig. 6, we plot the angular profiles of the (00) beam at the in-phase diffraction condition for various temperatures. Neither the FWHM nor the tails of the specular beam changes at any temperature up to 530 K. Therefore we have every

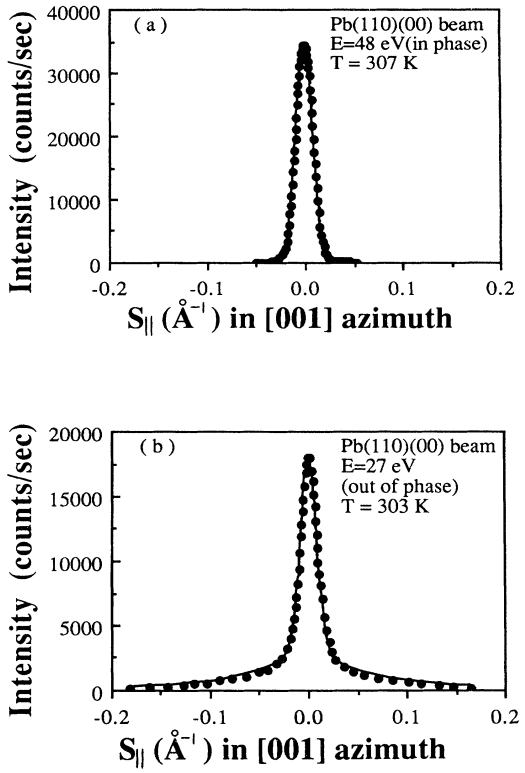

FIG. 3. The angular profiles of the (00) beam scanned in the [001] direction at the in-phase ($E=48$ eV) and the out-of-phase ($E=27$ eV) diffraction conditions, where the solid dots are the experimental data and the solid curves are the model fits based on the discussion in the text. $\mathbf{S}_{\parallel}$ is the momentum transfer parallel to the Pb(110) surface.

reason to believe that in our experiment neither the multiple scatterings nor the thermal diffuse scattering make a significant contribution to the change in the beam shape. It is a very important result which allows one to extract detailed information about the change of surface structure during the roughening transition.

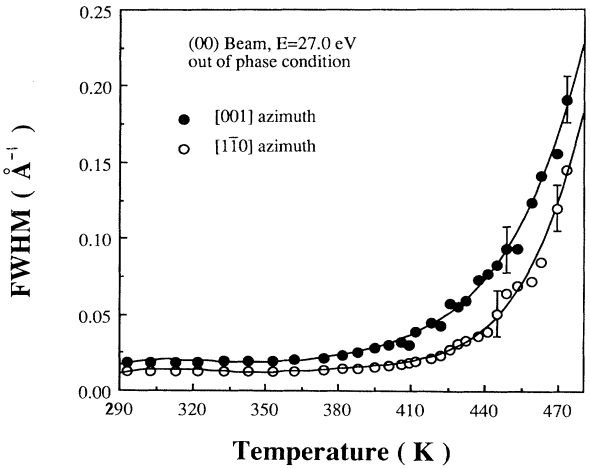

FIG. 4. The measured FWHM's of the (00) beam at the out-of-phase condition ($E=27$ eV) as a function of temperature. The solid curves are plotted as the guidelines.

C. Temperature-dependent peak intensity

The peak intensities of the (00), (10), and (01) beams as a function of temperature at both the in-phase (solid circles) and the out-of-phase (open circles) conditions are plotted in Fig. 7. At the in-phase condition, the peak intensity undergoes two changes with increasing temperature. Below $T\sim500$ K, the peak intensity behaves normally and the only change is a slight deviation of the peak intensity from the Debye-Waller decay starting at about 380 K, indicating an enhanced atomic vibration in the surface. In order to compare the atomic vibration amplitude, we assume (although it is not fully appropriate) that in two temperature regions, i.e., $295<T<380$ K and $380<T<500$ K, the peak intensity still follows the Debye-Waller decay but with different Debye-Waller factors. Using the formula

$$I_{\text{peak}}=I_0\exp(-2W) \tag{4}$$

with the Debye-Waller factor

$$2W=\langle(\mathbf{S}\cdot\mathbf{u})^2\rangle=\text{const}T\ , \tag{5}$$

we obtain the atomic vibrational amplitude perpendicular to the surface, $\langle u_{\perp}^2\rangle$, by fitting the experimental data of the (00) beam for each temperature region. At $T<380$ K, $\langle u_{\perp}^2\rangle/T=1.685\times10^{-4}$ Å^2 K^{-1}. While at $380<T<500$ K, $\langle u_{\perp}^2\rangle/T=3.913\times10^{-4}$ Å^2 K^{-1}, which is at least two times larger than that at $T<380$ K. Correspondingly, the mean-square vibrational amplitudes, $(\langle u_{\perp}^2\rangle)^{1/2}$, are 0.2248 Å at 300 K and 0.3956 Å at 400 K, which are 6.4% and 11.3%, respectively, of the nearest-neighbor atomic spacing (3.5 Å). Frenken *et al.* [10] have reported an anomalous expansion in the top layers of the Pb(110) surface at temperatures below 480 K using the high-energy ion channeling technique. It is closely related to the surface anharmonicity and therefore our result is consistent with their observation.

At $T>500$ K, the peak intensity drastically deviates from the Debye-Waller decay and changes much faster than it does at 380 K. The intensity falls to the background level when the temperature approaches 560 K, as seen in Fig. 7. The mean-square vibrational amplitude at 500 K is 0.4423 Å, 12.6% of the nearest-neighbor atomic distance. This dramatic decay of the peak intensity is due to the surface melting, which has been studied extensively in recent years by Frenken and van der Veen.[16]

At the out-of-phase condition, however, the peak intensity decays relatively faster than that at the in-phase condition in the temperature region below 500 K. As seen in Fig. 7(a), the peak intensity of the (00) beam at $E=27.0$ eV, which corresponds to the out-of-phase condition, falls more rapidly than that at $E=48.0$ eV, which corresponds to the in-phase condition (especially at $T>400$ K), even though the former has a smaller Debye-Waller factor due to its smaller momentum transfer. At about 480 K, the intensity drops to the background level. The intensities of the (10) and (01) beams also exhibit the same behavior, as seen in Figs. 7(b) and 7(c). Considering the fact that the dramatic change of the angular profile also occurs at this temperature region, we believe that the relatively faster decay of the peak in-

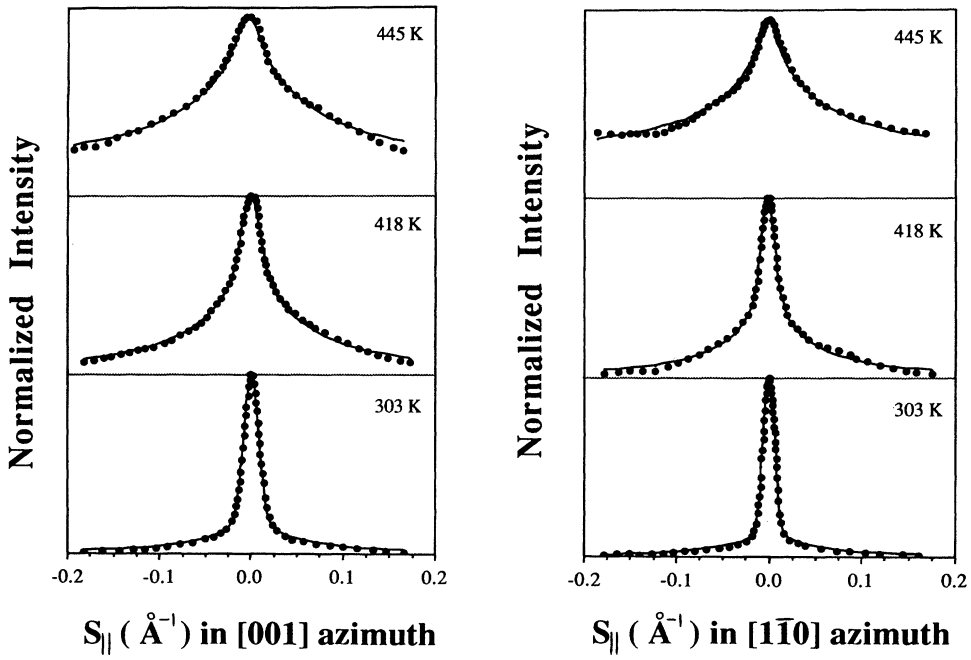

FIG. 5. The angular profiles of the (00) beam scanned along two azimuthal directions at the out-of-phase condition (E=27 eV) for various temperatures. The solid dots are the experimental row data and the solid lines are the fits based on Eq. (29) as explained in the text.

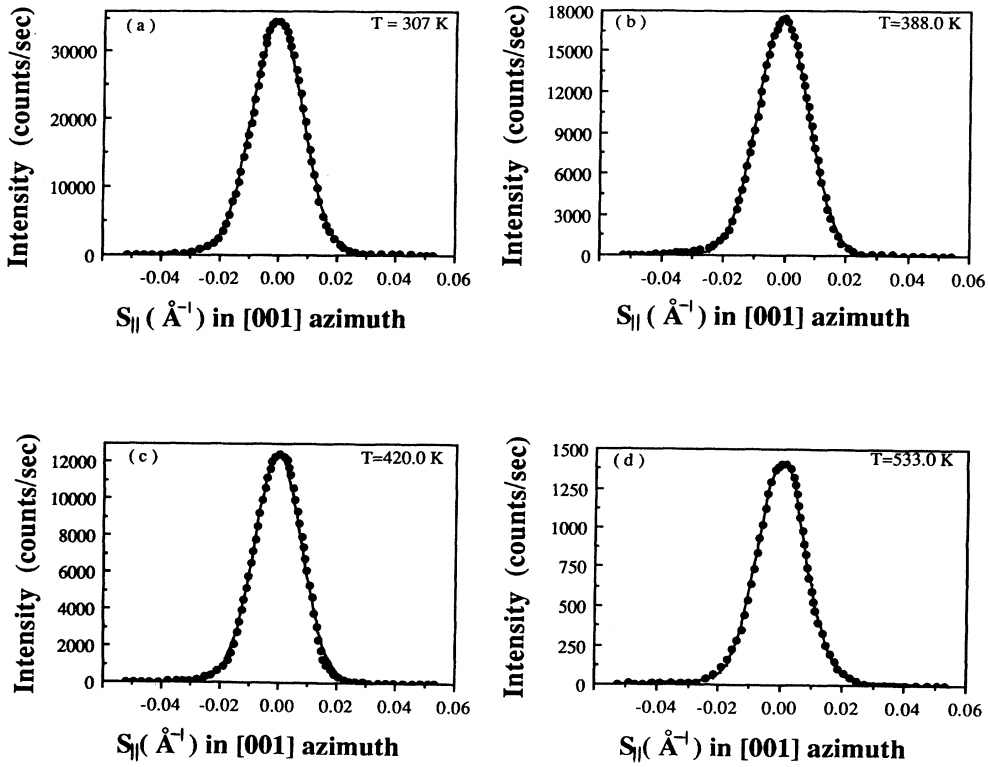

FIG. 6. The angular profiles of the (00) beam at the in-phase condition (E=48 eV) for various temperatures. The solid dots are the experimental raw data and the solid lines are the fits by a single Gaussian instrument response function.

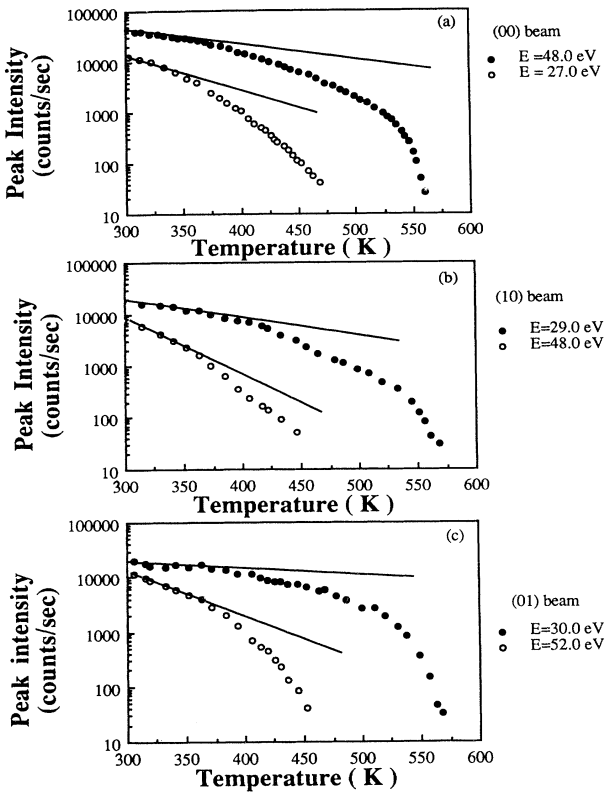

FIG. 7. The measured peak intensities of the (a) (00), (b) (10), and (c) (01) beams as a function of temperature at both the in-phase (solid circles) and out-of-phase (open circles) diffraction conditions. The straight lines in the figures indicate different decay rates between the in-phase and the out-of-phase conditions.

tensities at the out-of-phase condition is primarily due to the destructive interference between different atomic layers in the rough surface. This faster decay even starts at room temperature for which the surface roughening transition has not occurred. This indicates that the local step density continuously grows at low temperatures, which may be related to the surface preroughening. Unlike the analysis of the angular profile, a quantitative study of the peak intensity turns out to be difficult because of the complexities of the mixed effects due to surface anharmonicity, roughening, and even multiple scatterings. As discussed above, the line-shape analysis can effectively avoid this difficulty, which will be presented in Sec. IV.

As a brief conclusion, the surface roughening occurs between 400 and 500 K, while at about 380 K the surface exhibits an enhanced atomic vibration. The surface enhanced anharmonicity may be a possible driving mechanism for the roughening transition. A detailed discussion will be given in the final section.

III. THEORETICAL DESCRIPTION OF ROUGHENING TRANSITION IN fcc(110) SURFACES

A. Summary on Kosterlitz-Thouless (KT) surface roughening transition

The general features of the surface roughening phase transition have been discussed in the review papers by Weeks,[17] and by van Beijeren and Nolden.[18] The roughening transition is in the same universality class as that of the Kosterlitz-Thouless type[5] and is of infinite order. As T approaches T_R from below, the correlation length diverges very rapidly and remains infinite for $T \geq T_R$. The height-height correlation function $\langle [h(r)-h(0)]^2 \rangle$ diverges logarithmically as $r \to \infty$ at $T \geq T_R$, implying the interface width of the surface (called the "surface width") diverges at and above the roughening transition temperature.

The above conclusions were first drawn from a discrete Gaussian (DG) model by Chui and Weeks.[19] On the other hand, the body-centered solid-on-solid (bcSOS) model,[20] established by van Beijeren, also exhibits similar roughening features. The bcSOS model has the advantages that it is exactly solvable and can be directly applied to the fcc(110) surface.

The perfect (110) face of a fcc crystal is depicted in the top view and side view of Figs. 1(a) and 1(b), respectively. In this paper, we denote x and y to be in the $[1\bar{1}0]$ and [001] directions, respectively, as seen in Fig. 1(a). Its ABAB stacking structure consists of a body-centered tetragonal unit cell, as shown in Fig. 1(c). According to van Beijeren,[20] this configuration corresponds exactly to the bcSOS model. The bcSOS model was originally applied to an isotropic bcc(100) surface with a square unit mesh. For the fcc(110) surface, this model should be modified to include an anisotropic interaction associated with a rectangular unit mesh. The quantitative features of the roughening transition for this anisotropic bcSOS model are summarized[21] as follows.

(a) The roughening transition temperature T_R satisfies the equation

$$\Delta(T_R) = -1 , \tag{6}$$

with

$$\Delta(T) = (v^2+w^2-1)/2vw , \tag{7}$$

$$v = \exp(-J_x/k_B T) \quad \text{and} \quad w = \exp(-J_y/k_B T) . \tag{8}$$

J_x and J_y are the nearest-neighbor coupling constants along the $[1\bar{1}0]$ and [001] directions, respectively, in the rectangular unit mesh of the (110) surface. (For fcc bulk unit cell, J_y is the next-nearest-neighbor coupling constant.) Equation (6) can be simplified as

$$\exp(-J_x/k_B T_R)+\exp(-J_y/k_B T_R) = 1 . \tag{6'}$$

In the case of an isotropic bcSOS model, i.e., $J_x = J_y = J$, Eq. (6') can be reduced to $k_B T_R = J/\ln 2$.

(b) The height-height correlation function exhibits a logarithmic divergence as $|\mathbf{R}_{mn}| \to \infty$ at $T \geq T_R$. At $T < T_R$ the surface maintains a finite surface width ($\sim h_0$):

$$\langle [h(\mathbf{R}_{mn})-h(0)]^2\rangle \sim \begin{cases} 2h_0^2, & T<T_R \\ A(T)\ln\rho, & T\geq T_R \end{cases} , \quad (9)$$

where $\mathbf{R}_{mn}$ is the surface atom position, $\mathbf{R}_{mn}=m\hat{\mathbf{a}}+n\hat{\mathbf{b}}$ $(m,n=0,\pm1,\pm2,\ldots)$. $\hat{\mathbf{a}}$ and $\hat{\mathbf{b}}$ are the unit vectors along the $[1\bar{1}0]$ and [001] directions, respectively. (a is the nearest-neighbor spacing of a fcc crystal and $\sqrt{2}a=b$.) ρ is defined as

$$\rho^2=m^2+\epsilon^2 n^2 , \quad (10)$$

in which the anisotropic parameter ϵ is known exactly only at $T=2T_R$:

$$\epsilon=\exp[(J_x-J_y)/2k_B T_R] , \quad (11)$$

where we assume $J_x\geq J_y$. The capillary wave behavior, which exhibits the logarithmic divergence in Eq. (9), is one of the important characteristics of the KT transition. We shall call such a surface the "KT rough surface." Various other models[19,22,23] also predict a similar KT roughening behavior, except that the expressions for $A(T)$ are different [although at $T=T_R$, $A(T)$ has a universal value: $A(T_R)=2/\pi^2$]. In the case of the bcSOS model,

$$A(T)=(2/\pi^2)/[\tfrac{1}{2}-(1/\pi)\arcsin\Delta(T)] , \quad (12)$$

with $A(T_R)=2/\pi^2$.

It should be emphasized that the bcSOS model only takes into account the short-range and pairwise interactions among the surface atoms; this may not be reasonable for the low-index metal surfaces. Recently, Trayanov *et al.* [6] proposed a modified bcSOS model by redefining the coupling constants J_x and J_y in terms of the surface free energies of fcc(111), (100), and (110) faces. This consideration has included the many-body interactions and is more suitable for metal surfaces.[6]

B. Diffraction from the KT rough surface

We express the diffraction intensity from a crystalline surface as

$$I(\mathbf{S})=I_0(\mathbf{S})\sum_{m,n}\exp(i\mathbf{S}_\parallel\cdot\mathbf{R}_{mn}) \times\langle\exp\{i\mathbf{S}\cdot\mathbf{e}[h(\mathbf{R}_{mn})-h(0)]\}\rangle , \quad (13)$$

where $\mathbf{S}$ is the total momentum transfer, $\mathbf{S}_\parallel$ is its component parallel to the (110) surface, $I_0(\mathbf{S})$ is the atomic form factor, and $\mathbf{e}$ is the elementary translation vector between neighboring terraces.[24] The summation is over the two-dimensional atomic positions of the surface. In the case of a fcc(110) surface, assuming only the single step height is allowed, we can express $\mathbf{e}$ as

$$\mathbf{e}=\pm\hat{\mathbf{a}}/2\pm\hat{\mathbf{b}}/2+\mathbf{t} \quad (14)$$

and

$$\mathbf{S}\cdot\mathbf{e}=\begin{cases} S_\perp t, & \text{for the (00) beam} \\ S_\perp t\pm S_x a/2=S_\perp t\pm\pi, & \text{for the (01) beam} \\ S_\perp t\pm S_y b/2=S_\perp t\pm\pi, & \text{for the (10) beam} \end{cases} , \quad (15)$$

where S_x and S_y are the momentum transfers parallel to the $[1\bar{1}0]$ and [001] directions, respectively, and $\mathbf{t}$ the step vector along the surface normal. Actually, $\mathbf{S}\cdot\mathbf{e}$ is just the phase difference φ for (00), (10), and (01) beams, as given in Eq. (2). The thermal average of Eq. (13) can be obtained by the Gaussian approximation,[22] i.e.,

$$\langle\exp\{i\mathbf{S}\cdot\mathbf{e}[h(\mathbf{R}_{mn})-h(0)]\}\rangle =\exp\{-[\mathbf{S}\cdot\mathbf{e}]^2\langle[h(\mathbf{R}_{mn})-h(0)]^2\rangle/2\} , \quad (16)$$

where $[\mathbf{S}\cdot\mathbf{e}]$ means $\mathbf{S}\cdot\mathbf{e}$ mod 2π such that $-\pi<[\mathbf{S}\cdot\mathbf{e}]<\pi$. Replacing the summation in Eq. (13) by an integral as an approximation and combining Eq. (13) with Eq. (9), we can calculate the diffracted intensity which is the 2D Fourier transformation of Eq. (16):

$$I(\mathbf{S})\propto\begin{cases} \delta(\mathbf{S}_\parallel\pm\mathbf{G}_{hk})\exp(-h_0^2[\mathbf{S}\cdot\mathbf{e}]^2), & T<T_R \\ |\mathbf{Q}|^{-[2-n(T)]}, & T\geq T_R \end{cases} , \quad (17)$$

where

$$|\mathbf{Q}|^2=(S_x-2\pi h/a)^2+(S_y-2\pi k/b)^2/\epsilon^2 \quad (18)$$

for various (hk) order beams $(h,k=0,\pm1)$ and

$$n(T)=[\mathbf{S}\cdot\mathbf{e}]^2 A(T)/2 . \quad (19)$$

$\mathbf{G}_{hk}$ is the two-dimensional reciprocal lattice vector for the (hk) beam.

Although the surface width h_0 in Eqs. (9) and (17) does not have an explicit form in the bcSOS model, it is in general a monotonic increasing function of temperature (due to the thermal excitation of local defects).

At $T<T_R$ the Bragg intensity has a δ-function profile with an additional Debye-Waller-like factor, $\exp(-h_0^2[\mathbf{S}\cdot\mathbf{e}]^2)$, corresponding to the coherent diffraction from the long-range ordered flat surface with a finite surface width h_0. As the temperature is raised, the surface width gradually grows with the thermal generation of defects and therefore the intensity of the δ-like peak continues to decay. This explains why as the temperature is raised to T_R from below, the anti-Bragg peak intensity falls faster than that expected from the thermal vibration, as observed in our experiment (Fig. 7). At $T\geq T_R$, the surface width diverges. As a result, the δ-like peak disappears and is replaced by the power-law line shape which corresponds to the diffraction from the KT rough surface.

In the case of the out-of-phase diffraction conditions, i.e., $\mathbf{S}\cdot\mathbf{e}=\pm\pi,\pm3\pi\ldots$, the exponent

$$n(T)=[\tfrac{1}{2}-(1/\pi)\arcsin\Delta(T)]^{-1} . \quad (20)$$

Specifically, as $T=T_R$,

$$n(T_R)=1 . \quad (21)$$

C. Considerations of short-range roughness

As mentioned earlier, Eq. (9) only exhibits the asymptotic behavior of surface height-height correlation function and therefore the diffraction intensity, i.e., Eq. (17), only reflects the long-range character in the surface.

Practically, Eq. (17) alone may not be used to interpret the entire experimental data because the short-range roughness always exists and it makes a certain contribution to the diffraction profile. The short-range roughness, reflecting the local step structure at both $T<T_R$ and $T\geq T_R$, manifests itself in the tail part (larger $S_\parallel$, away from the central Bragg peak) of the angular profile and therefore contributes a broad diffuse background, which may affect the intensity of the power-law tail. This diffuse background, usually appearing as a Lorentzian shape, has been observed in our experiment and has been reported also in many cases.[1,3,24] The bcSOS model as well as other models do not provide an explicit solution to the short-range correlation function. Hence establishing a phenomenological model may be an alternative approach. Since the short-range roughness does not signify the divergence of the surface width and roughening transition, a surface with a finite width of defect layers is a simple model to describe the low-temperature surface ($T<T_R$). The simplest model, a two-level system,[25,26] shows that the diffracted profile consists of a central δ function superimposed on a broadened Lorentzian diffuse background. A similar result can be obtained for a finite, but multilevel system (as long as the surface width is still finite),[26] which is still consistent with the experimental observations. As mentioned above, one possible origin of this Lorentzian diffuse background may be caused by a surface preroughening effect.[15]

We therefore phenomenologically add a Lorentzian term to Eq. (17), i.e.,

$$I(\mathbf{S})\propto\begin{cases}\mathbf{R}_0(T)\delta(\mathbf{S}_\parallel\pm\mathbf{G}_{hk})+L(\mathbf{S}_\parallel\pm\mathbf{G}_{hk}), & T<T_R \quad (22a)\\ \mathbf{R}(T)|\mathbf{Q}|^{-[2-n(T)]}+L(\mathbf{S}_\parallel\pm G_{hk}), & T\geq T_R, \quad (22b)\end{cases}$$

where the Lorentzian function $L(\mathbf{S}_\parallel)$ has two different versions:

$$\mathbf{L}(\mathbf{S}_\parallel)=\begin{cases}(1-\xi)^2[1+\xi^2-2\xi\cos(\mathbf{S}_\parallel\cdot\mathbf{a})]^{-1} \text{ (discrete surface model}^{25}) & (23a)\\ [1+(|\mathbf{S}_\parallel|/\sigma_L)^2]^{-1} \text{ (continuous surface model}^{26}). & (23b)\end{cases}$$

The parameter ξ in Eq. (23a) is a function of the step density and $0<\xi<1$. In principle, the discrete surface model, in which the diffraction is from the discrete atoms in a terrace, is more rigorous for describing the short-range behavior. In reality, the difference between the two models is quite small. This is because the FWHM of the Lorentzian usually is small, compared with the dimension of the first Brillouin zone (typically $\sim 10\%$). Therefore the short-range order and the average terrace size are still large enough so that the discrete atomic nature of the terrace can be ignored. For the discrete surface version, the corresponding FWHM is equal to $2\sigma'_L$, where

$$\sigma'_L=\frac{1}{a}\arccos\left[1-\frac{(1-\xi)^2}{2\xi}\right].$$

If σ'_L is small, ξ will be close to 1, and this results in the approximation

$$\sigma'_L\approx\frac{1-\xi}{a\sqrt{\xi}}.$$

The same result can be obtained by expanding $\cos(\mathbf{S}_\parallel\cdot\mathbf{a})\approx 1-(\mathbf{S}_\parallel\cdot\mathbf{a})^2/2$. Thus the discrete model version can be simply transformed into the continuous model version. For both versions, the width of the Lorentzian function is approximately proportional to the local step density in the surface.

The physical meaning of Eq. (22) can be summarized as follows: Below T_R, the Lorentzian width increases with temperature. This is due to the continuous excitation of the local steps. The surface is still "flat" and maintains a long-range order. The ratio $R_0(T)$ of the δ component to the Lorentzian term mainly depends on both the surface width h_0 and the step density. This ratio decreases monotonically as the temperature approaches T_R. For $T\geq T_R$, the δ component evolves into the power-law line shape which superimposes on a broader Lorentzian diffuse background [with a ratio $R(T)$].

D. Convolution of the diffracted intensity with the instrument response function

The fitting of the experimental profile will be performed by using Eq. (22) convoluted with the instrument response function. In our HRLEED system, the instrument response function can well be described as a Gaussian profile. At low temperatures $T<T_R$, the convolution of Eq. (22a) is simply a sum of a Gaussian function and a convoluted Lorentzian function (denoted as "$G+G*L$").

For $T\geq T_R$, the convolution of the power-law function is more involved. It has been shown by Dutta and Sinha[27] that the 2D convolution of an isotropic power-law function, $|\mathbf{Q}|^{-[2-n(T)]}$, with a 2D Gaussian function of width σ, is proportional to the Kummer function:

$$\exp(-Q^2/\sigma^2)*|\mathbf{Q}|^{-(2-n)}\propto\phi(1-n/2;1;-Q^2/\sigma^2), \quad (24)$$

where the Kummer function ϕ is defined as

$$\phi(\alpha;\beta;z)=\sum_{m=0}^{\infty}\frac{\Gamma(\alpha+m)\Gamma(\beta)}{\Gamma(\alpha)\Gamma(\beta+m)}\frac{z^m}{m!}.$$

Here $\Gamma(x)$ is the gamma function.

However, for the anisotropic system we are studying here, the convolution turns out to be slightly more complicated. The Taylor-series expansion with respect to the anisotropic factor gives an explicit form for this convoluted angular profile (along $x\equiv[1\bar{1}0]$ and $y\equiv[001]$ direc-

tions, respectively):

$$I(S_x,0)\propto C_x^{-(2-n)}\sum_{j=0}^{\infty}\frac{\Gamma(j+\frac{1}{2})\Gamma(j+1-n)}{(j!)^2}\eta_x^j \times\phi\left[j+1-\frac{n}{2};j+1;-\frac{S_x^2}{\sigma_x^2}\right],$$

and

$$I(0,S_y)\propto C_y^{-(2-n)}\sum_{j=0}^{\infty}\frac{\Gamma(j+\frac{1}{2})\Gamma(j+1-n)}{(j!)^2}\eta_y^j \times\phi\left[j+1-\frac{n}{2};j+1;-\frac{S_y^2}{\sigma_y^2}\right], \tag{25}$$

where $C_x=\sigma_x a$, $C_y=\sigma_y b/\epsilon$, and σ_x and σ_y are the Gaussian widths of the instrument response along the $[1\bar{1}0]$ and [001] directions, respectively. ϵ is the anisotropic parameter defined in Eqs. (10) and (11). The anisotropic factor η's are defined as

$$\eta_x=1-(C_x/C_y)^2=1-(\epsilon\sigma_x a/\sigma_y b)^2, \tag{26a}$$

$$\eta_y=1-(C_y/C_x)^2=1-(\sigma_y b/\epsilon\sigma_x a)^2. \tag{26b}$$

If $\sigma_x a=\sigma_y b$ and $\epsilon=1$, one has $\eta_x=\eta_y=0$, so that the anisotropy no longer exists and Eq. (25) is just the isotropic solution, Eq. (24).

As is known, the Kummer functions in Eq. (25) have an asymptotic form[28] at large Q:

$$\phi(j+1-n/2;j+1;-Q^2/\sigma^2)\sim(Q/\sigma)^{-(2j+2-n)}. \tag{27}$$

As a result, by retaining the lowest-order term, the tail part in the intensity expression, Eq. (25), exhibits a power-law behavior with the exponent $(2-n)$, i.e.,

$$I(S_x,0)\sim(S_x a)^{-(2-n)} \text{ and } I(0,S_y)\sim(S_y b/\epsilon)^{-(2-n)}, \tag{28}$$

which are independent of the instrument response function.

Equation (25) is the series expansion in terms of the order of the anisotropic factors, $\eta_x=1-(\epsilon\sigma_x a/\sigma_y b)^2$ and $\eta_y=1-(\sigma_y b/\epsilon\sigma_x a)^2$, respectively, for the $[1\bar{1}0]$ and [001] directions. From Eq. (27), we see that only the zeroth-order term (i.e., $j=0$) retains the power-law line shape with the minimum exponent $(2-n)$. Therefore it is a reasonable approximation to retain the zeroth-order term in the intensity expression, Eq. (25). This zeroth-order intensity has a form similar to that of the isotropic solution Eq. (24):

$$I(S_x,0)\propto(\sigma_x a)^{-(2-n)}\phi(1-n/2;1;-S_x^2/\sigma_x^2),$$

$$I(0,S_y)\propto(\sigma_y b/\epsilon)^{-(2-n)}\phi(1-n/2;1;-S_y^2/\sigma_y^2).$$

The higher-order terms ($j\geq 1$), which have a power-law shape of larger exponent $(2j+2-n)$, as seen in Eq. (27), drop more rapidly in the tail part. Therefore these terms can be quantitatively treated as a small diffuse background and be included in the Lorentzian part that corresponds to the short-range roughness.

Combined with the scattering intensity due to the short-range roughness, at $T\geq T_R$, the diffraction intensity should be expressed as the sum of a Kummer function and a convoluted Lorentzian function (denoted as "$K+G*L$"). In conclusion, the diffraction intensity, Eq. (22), after the convolution, can be finally written as

$$I(S_i)\propto\begin{cases}R_{0i}\exp[-(S_i/\sigma_i)^2]+G(S_i/\sigma_i)*L(S_i), & T<T_R \quad (29a)\\ R_i\phi(1-n/2;1;-S_i^2/\sigma_i^2)+G(S_i/\sigma_i)*L(S_i), & T\geq T_R \quad (29b)\end{cases}$$

where $i=x,y$ and the Gaussian function $G(z/\sigma)=\pi^{-1/2}\sigma^{-1}\exp[-(z/\sigma)^2]$. In a flat surface the ratio of the Gaussian to the Lorentzian, R_{0i}, depends on the short-range roughness characterized by the local step density and the surface width. However, in the rough surface, the ratio R_i of the Kummer function to the Lorentzian is not only a function of the short-range roughness but also the KT surface roughness which is characterized by the exponent $n(T)$. Besides, both R_{i0} and R_i are anisotropic in the x and y directions (R_i depends on the anisotropy ϵ).

IV. LINE-SHAPE ANALYSIS

We use the angular profile at the in-phase condition as the effective instrument response function, which is fitted very well, as shown in Fig. 3(a), by a single Gaussian function with the FWHM's equal to 0.014 ± 0.002 Å^{-1} and 0.019 ± 0.002 Å^{-1} along the $[1\bar{1}0]$ and [001] azimuths, respectively.

A. Low-temperature line shape

As discussed in Sec. III, the low-temperature angular profile ($T<T_R$) should be fitted by the sum $G+G*L$, as expressed in Eq. (29). In the fit, the Gaussian width σ_G, Lorentzian width σ_L, and the ratio R_{0i} are the adjustable parameters.

The room-temperature line shape at the out-of-phase condition, as seen in Fig. 3(b), is fitted quite well by the calculation. The Gaussian component has a peak width almost the same as that at the in-phase condition, indicating that it is the δ component diffracted from the flat surface with a long-range order. The Lorentzian FWHM's ($=2\sigma_L$) are 0.150 ± 0.005 Å^{-1} along both $[1\bar{1}0]$ and [001] azimuths. The ratio R_0 of the Gaussian to Lorentzian is 87% and 82% along the $[1\bar{1}0]$ and [001] directions, re-

spectively.

The fitting parameters as a function of temperature are plotted in Fig. 8. For a comparison, we have also fitted the higher-temperature profiles using the same fitting procedure, i.e., by Eq. (29a). Below $T=400$ K, the Gaussian width has no significant change while the Lorentzian component continues to broaden. The ratio $R_0(T)$, as seen in Fig. 8(c), decays slowly at $T<380$ K. All of these indicate that in this temperature region the surface is flat but the local step density and the surface width slowly increase with temperature.

At $T\sim380$ K, $R_0(T)$ starts to decay much faster. This implies that the surface width increases and the local steps start to generate quickly into the deeper surface layers. The Gaussian component, on the other hand, also begins to broaden significantly at $T\sim410$ K, suggesting that the δ component, which represents the long-range order of the flat surface, no longer exists at this temperature. It is more convincing to see this point by referring the integrated intensity as a function of temperature. As plotted in Fig. 9, the integrated intensity of the δ component, which is calculated from the $G+G^*L$ fit, decays quickly and drops to the zero level at $T\sim410$ K, while the total integrated intensity changes slowly. The total integrated intensity should only depend on the surface atomic vibration (the Debye-Waller effect and the anharmonicity).

The broadening of the Gaussian function signifies not only the disappearance of the δ component but also the emergence of the power-law line shape. This is because the power-law line shape, after convolution with the Gaussian resolution function, still has a Gaussian portion[28] in the central part but its FWHM is broader than that of the instrument response. It has been shown[6] that in the case of $n=1$, the convoluted power-law shape broadens about 60% if the Gaussian instrumental response has a 0.02 Å^{-1} FWHM. Therefore the broadening of the δ component suggests that the fitting of $G+G^*L$ may not be appropriate anymore and should be replaced by a sum of $K+G^*L$, i.e., Eq. (29b), which would be consistent with both the experiment and the theory.

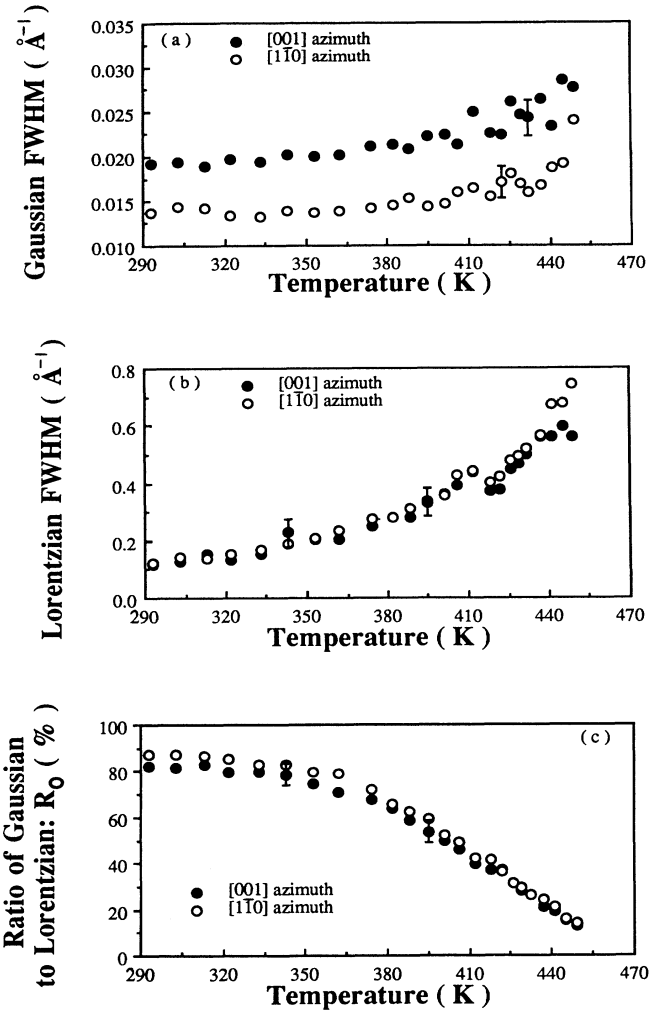

FIG. 8. Plots of fitting parameters used in the $G+G^*L$ fit vs temperature: (a) the Gaussian FWHM σ_G, (b) Lorentzian FWHM, and (c) the ratio R_0. The solid curves are guidelines to the eyes.

B. High-temperature line shape

Before the $K+G^*L$ fit scheme is performed, we employ a more intuitive way to display the change of the tail part of the measured angular profile as a function of temperature. Figure 10 shows the log-log plots of the tail part of the (00) beam (out-of-phase condition) in the [1$\bar{1}$0] azimuth at various temperatures. The data shown in Fig. 10 are raw data and they extend from 0.03 to 0.09 Å^{-1}, which are $\geq 2.5\sigma_G$ so that the influence of the instru-

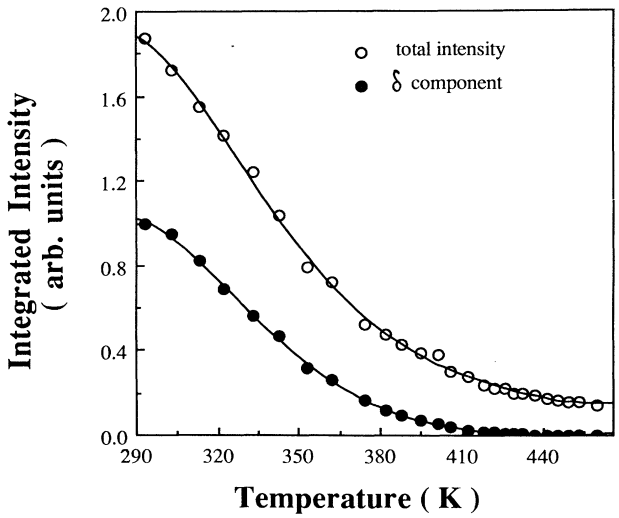

FIG. 9. Temperature dependence of integrated intensities of the (00) beam at the out-of-phase condition ($E=27$ eV). The integration is carried out in the [1$\bar{1}$0] direction. The integrated intensity of the δ component is determined from R_0 by means of the $G+G^*L$ fit.

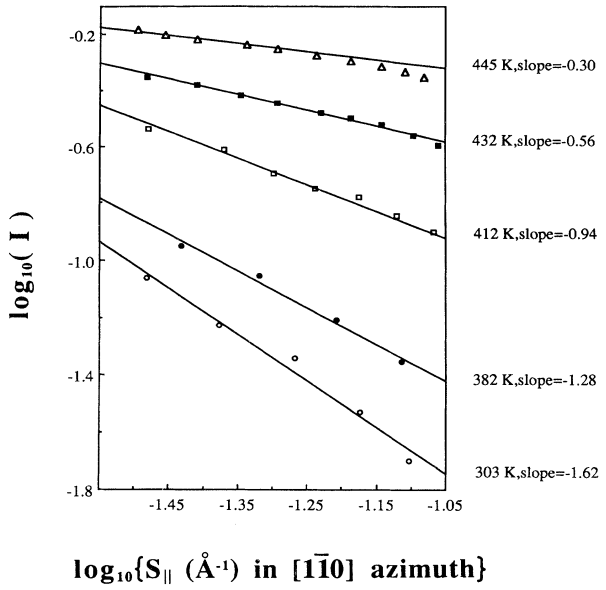

FIG. 10. $\mathrm{Log}_{10}(I)$ vs $\log_{10}(\mathbf{S}_{\|})$ (out-of-phase condition) in the $[1\bar{1}0]$ direction at various temperatures. These experimental raw data extend from 0.03 to 0.09 Å^{-1}. The slope for each line shape is equal to $-(2-n)$. As the exponent $n(T)$ approaches 1, the KT roughening transition occurs. The roughening temperature T_R is around 412 K as shown in the figure.

mental response can be safely ignored.[29] The data at $|\mathbf{S}_{\|}|>0.09$ Å^{-1} (corresponds to $\log_{10}|\mathbf{S}_{\|}|>-1.05$) are affected by the Lorentzian diffuse background due to the local steps (short-range roughness) and therefore should not be considered here. According to Eq. (28), the slope for each line shape (which exhibits a straight line in the log-log plot), is given by $-(2-n)$. At room temperature, n is a small number. The change of the slope with temperature indicates that the exponent $n(T)$ starts to increase as $T>380$ K. The $n(T)$ reaches 1 at about 410 K, which is close to the roughening temperature. $n(T)$ continues to grow as the temperature is raised further. Similar plots have been obtained for profiles along the [001] azimuth.

However, we have to point out that the way to estimate the exponent $n(T)$ through the log-log plot of the raw data may not be accurate because the diffuse background may affect the tail intensity of the profile. Especially at low temperatures, this influence is stronger. At $T=303$ K, for example, the slope gives $n\approx 0.4$, which is too high for the flat surface. Actually, at $T<T_R$, the major part in the tail is the Lorentzian shape while at $T\geq T_R$ the power-law component becomes the dominant part in the tail.

Therefore a more quantitative method to determine the exponent $n(T)$ is to fit the angular profile in terms of $K+G^*L$, which can separate the power-law component from the Lorentzian diffuse background, as given in Eq. (29b). On the other hand, as the exponent $n\to 0$, the Kummer function is just the Gaussian function with the same width as the instrumental response, i.e.,

$$\phi(1-n/2;1;-Q^2/\sigma^2)\to G(Q/\sigma)=\exp(-Q^2/\sigma^2)\ ,$$

as $n\to 0$.

Consequently, as $n\to 0$, $K+G^*L\to G+G^*L$. That is, if n is small, these two fits, $K+G^*L$ and $G+G^*L$, have no significant difference. Therefore this property of the Kummer function allows us to extend the $K+G^*L$ fit to the line shape at low temperatures (at $T<T_R$, n is usually small). In the fitting, the adjustable parameters are chosen to be the exponent $n(T)$, Lorentzian width σ_L, and the ratio R. The result of fitting is shown as follows.

The comparison of the quality of fit, $\chi^2=\Sigma(I_{\mathrm{exp}}-I_{\mathrm{fit}})^2$, between $K+G^*L$ fits and $G+G^*L$ fits is demonstrated in Fig. 11, in which the relative difference of the quality of fit, i.e., $\Delta=(\chi^2_{G+G^*L}-\chi^2_{K+G^*L})/\chi^2_{K+G^*L}$, is plotted as the function of temperature. At low temperatures ($T\leq 380$ K), $\Delta\approx 0$ (as seen in Fig. 11), i.e., the two fits are the same, which is not surprising because in this temperature region, n is small. However, for $T>380$ K, the result obtained from $K+G^*L$ fits is much better than that by the $G+G^*L$ fits. As shown in Fig. 11, Δ increases from 0% at $T<380$ K to about 200% at $T\sim 410$ K. The quality of $K+G^*L$ fits, $\chi^2_{K+G^*L}$, maintains as a constant for all temperatures, which is about 0.0005 ± 0.0002. The fit by $G+G^*L$ becomes worse at $T>380$ K and $\chi^2_{G+G^*L}$ increases at least by a factor of 3 at $T\sim 410$ K. The fitting of the angular profiles according to the $K+G^*L$ fits has been plotted as solid curves in Fig. 5 in order to compare it with the experimental raw data. The above comparison of fits indicates that, at $T>380$ K, the appearance of the power-law line shape is the major reason which causes the poor fit by using the $G+G^*L$ scheme.

At $T\leq 380$ K, the Lorentzian width σ_L and the ratio R_0, fitted by $K+G^*L$, change similarly compared to that by $G+G^*L$ in the same temperature region. For

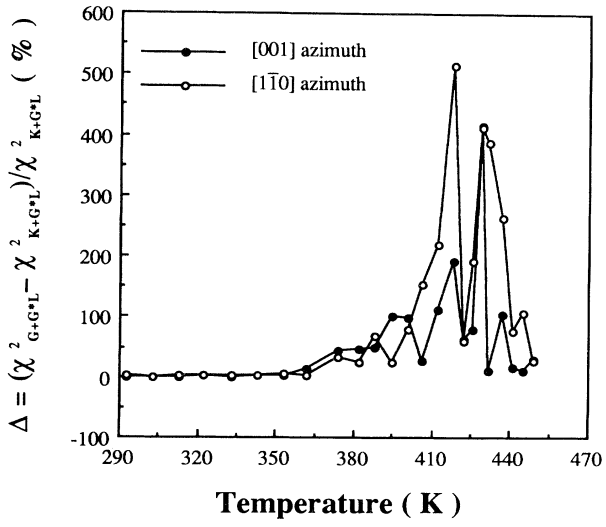

FIG. 11. The relative difference for the quality of fit χ^2, $\Delta=(\chi^2_{G+G^*L}-\chi^2_{K+G^*L})/\chi^2_{K+G^*L}$, is plotted as a function of temperature for two azimuthal directions. Note that Δ is very small at $T\leq 380$ K and becomes larger at $T\sim 410$ K.

$T > 380$ K, they change slowly, only showing a slight difference from that at $T = 382$ K. This indicates that the short-range roughness has reached saturation at $T \sim 380$ K, and the long-range roughening effect starts to dominate the change in the surface.

Figure 12 is a plot of the exponent n extracted from the above-mentioned fits as a function of temperature. Below 380 K, n remains constant and is a very small number. For $T > 380$ K, n starts to increase with temperature. The transition temperature occurs at 415 ± 10 K where $n \approx 1$. This conclusion is also consistent with the integrated intensity plot shown in Fig. 9, in which the integrated intensity of the δ component drops to zero at ~ 410 K. On the other hand, as shown in Fig. 4, the FWHM's of the angular profiles for the (00) beam are 0.0236 and 0.0429 Å^{-1} along the $[1\bar{1}0]$ and [001] azimuths, respectively, at $T = 422$ K. The increases are about 60% and 120%, respectively, compared with that at low temperatures. As mentioned earlier, the quantitative calculation has shown that the FWHM would increase about 60% at $n = 1$. The FWHM in the $[1\bar{1}0]$ azimuth agrees well with this 60% prediction while in the [001] direction the 120% increase in the FWHM is twice as much as that by the prediction. This "overbroadening" may be due to the anisotropic effect during the surface roughening transition, which will be discussed in Sec. IV C.

The measured transition temperature agrees remarkably well with a recent molecular-dynamics calculation.[30] This study predicts that the roughening should occur at $T_R = 0.7 T_m$ for a fcc(110) surface. For lead, $0.7 T_m = 420$ K.

According to the bcSOS model, as the temperature approaches to T_R from above, the exponent $n(T)$ can be expanded from Eq. (20) as

$$n(T) = 1 + C(T - T_R)^{1/2}, \quad T \geq T_R \ , \tag{30}$$

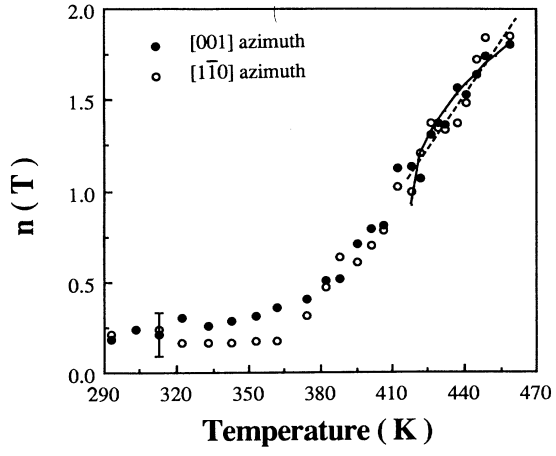

FIG. 12. The exponent $n(T)$ extracted from the $K + G^* L$ fits as a function of temperature. The solid curve is the fit by Eq. (30) and the dashed curve represents the fit by a straight line. These two curves do not exhibit a significant difference in the temperature region shown in the figure.

where the constant C is easy to calculate from Eqs. (12) and (6'), which are only functions of J_x and J_y. However, the increase of $n(T)$ at $T > T_R$, as shown in Fig. 12, is quicker. As a result, the fit of $n(T)$ by Eq. (30) (C is the only adjustable parameter) exhibits no significant difference from that by using a linear relation: $n(T) \propto (T - T_R)$. The fit of Eq. (30) and the linear fit are plotted as solid and dashed curves, respectively, in Fig. 12. An explanation regarding this is that the data we obtained are only in a small temperature region (from 415 to 455 K). This range may not be large enough to exhibit a significant deviation of Eq. (30) from a straight line. It is not possible to measure the angular profile at the out-of-phase condition for $T > 460$ K where the peak intensity has reached the background level in our experiment.

C. The anisotropy of the roughening transition

The anisotropy of the roughening transition in the Pb(110) surface is quite obvious from Fig. 4, in which the measured FWHM along the [001] azimuth broadens earlier than that along the $[1\bar{1}0]$ azimuth, as the temperature is close to T_R. At $T = 422$ K, the FWHM of the [001] direction has increased about 120% while that of the $[1\bar{1}0]$ direction only increased about 60%.

Figure 13 shows the log-log plots of the tail intensity of

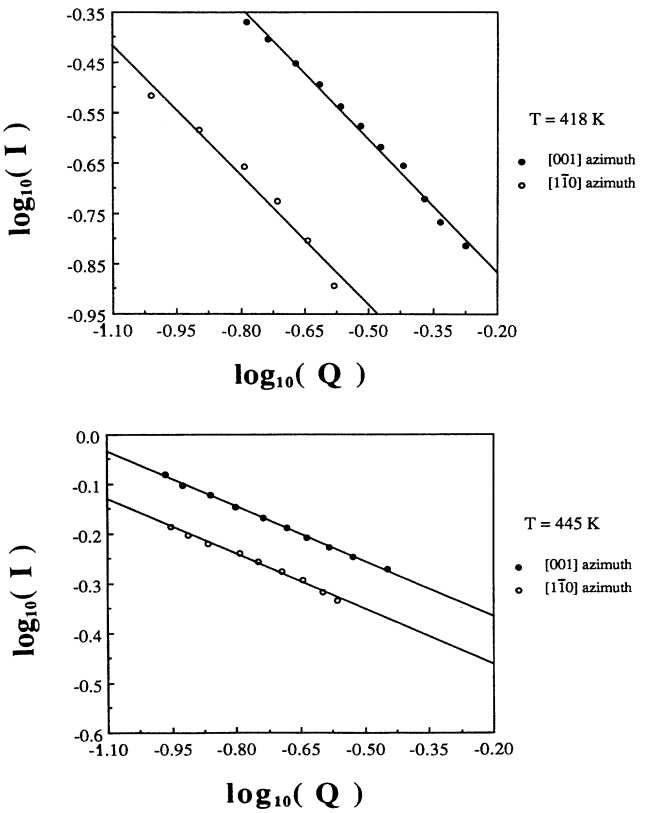

FIG. 13. The log-log plot of the (00) beam (out-of-phase condition) for [001] and $[1\bar{1}0]$ azimuths using the new scale: $S_x a = S_y b = Q$. The relative shift of the two curves is a direct measure of the anisotropy parameter ϵ as discussed in the text.

the angular profiles in both [001] and [1$\bar{1}$0] directions at $T=418$ and 445 K. In order to extract the anisotropy parameter ϵ, we have rescaled the scale with respect to $S_x a$ and $S_y b$, respectively, in the plots. From Eq. (28) for large S_x and S_y, we let $I(S_x,0)=I_x$ and $I(0,S_y)=I_y$. One has

$$\log_{10}(I_x)=-(2-n)\log_{10}(S_x a)+\text{const} ,$$

$$\log_{10}(I_y)=-(2-n)\log_{10}(S_y b)+(2-n)\log_{10}(\epsilon)+\text{const} .$$

In the new scale, letting $S_x a=S_y b=Q$, we obtain

$$\log_{10}(I_y)-\log_{10}(I_x)=(2-n)\log_{10}(\epsilon) .$$

Therefore ϵ can be obtained from the relative shift between the log-log plots along these two directions. As seen in Fig. 13, such a shift at $T=445$ K is smaller than that at 418 K, indicating that the anisotropy decreases rapidly with temperature. The ϵ's are then extracted from the plots, which are 2.38 at 418 K and 1.79 at 445 K (remember that for an isotropic case, $\epsilon=1$). Using the value of ϵ at $T=418$ K, we can estimate the coupling constants J_x and J_y. Assuming approximately $\epsilon=\exp[(J_x-J_y)/k_B T]$ (rigorously speaking, it should only hold for $T=2T_R$), and using Eq. (6'), we obtain $J_x\approx 1.22 k_B T_R$ and $J_y\approx 0.35 k_B T_R$. Hence the ratio $J_x:J_y\approx 3.46:1$. This ratio indicates that the interaction along the [1$\bar{1}$0] direction is much stronger than that in the [001] direction and therefore it exhibits a large anisotropic interaction in the surface. The significance of this anisotropy will be discussed in the next section.

V. SUMMARY AND DISCUSSION

We have presented a detailed analysis for the HRLEED experimental data collected from the Pb(110) surface. The line-shape analysis based on the well-developed roughening theory indicates that this low-index metal surface undergoes a clear surface roughening phase transition at $T_R\sim 415$ K, which is ~ 185 K below the bulk melting temperature.

In addition, the measurement also indicates that an enhanced surface atomic vibration occurs at about 380 K, just below the roughening transition temperature, which suggests the surface enhanced anharmonicity may be a possible driving mechanism for the roughening transition. The sequence of the instabilities in the Pb(110) surface described in the present experiment is derelaxation and anharmonicity (~ 380 K)$\rightarrow$ surface roughening (~ 415 K)$\rightarrow$surface melting (~ 560 K)$\rightarrow$bulk melting (~ 600.7 K). One instability drives the next until the bulk melts.

The modified bcSOS model, proposed by Trayanov *et al.*, [6] suggests that the anisotropic local defects, such as pieces of (111) and (100) facets, play a leading role in the roughening transition on a fcc(110) metal surface. The thermal generation of a small piece of (111) facet is easier than that of (100) facet and the surface tends to form the $(1\times n)$ missing rows $(1\times 2, 1\times 3, \ldots, 1\times n, \ldots)$ or steps parallel to the [1$\bar{1}$0] direction. The critical quantities, which determine whether or not the roughening transition could occur, have been given[6] by

$$\sigma=1.2247\sigma_{111}-\sigma_{110}$$

and by the anisotropy parameter ν^{-1}:

$$\nu^{-1}=(1.4142\sigma_{100}-\sigma_{110})/\sigma=J_x/J_y ,$$

where σ_{111}, σ_{100}, and σ_{110} are the surface free energies in the (111), (100), and (110) faces, respectively. Usually, $\sigma_{111}<\sigma_{100}<\sigma_{110}$. If σ is mildly positive and the anisotropy parameter ν^{-1} is large, the roughening transition could occur while if σ is positive but large and then ν^{-1} is not large enough, the roughening would not be favored. The quantity σ, which reflects the energetic cost of the generation of the (111) facet, depends on the ratio of the surface energies: $\sigma_{111}:\sigma_{110}$. For the Pb(110) surface, at $T<300$ K the large inward relaxation of the top layer (as has been reported previously,[11,12] the top layer contraction is about $15.4\pm 2.5\%$) results in a highly stable (110) surface. Its surface free energy σ_{110} is much lower than that without contraction. As a result, at low temperatures the large top layer relaxation leads to a smaller anisotropy parameter ν^{-1} and a larger σ value. For such ν^{-1} and σ values, the Pb(110) surface would not undergo a roughening transition. However, the observed anomalous expansion of the top layer at $T\geq 380$ K, which is followed by the large anharmonicity, almost eliminates the contraction. Under this dramatically changed situation, the "derelaxation" significantly increases the free energy σ_{110} and hence the relative energetic cost to form the (111) facet defects and the steps becomes much less than that at low temperatures. Consequently, this "derelaxation" drastically changes the critical quantities, σ and ν^{-1}, such that the roughening is favored and leads to the roughening transition at $T\sim 415$ K.

The above qualitative discussion shows that the surface anharmonicity plays a key role in the Pb(110) surface roughening transition. A similar situation was also observed in the Ni(110) surface.[3] More quantitative study on this "derelaxation" induced anisotropic roughening transition is desirable.

ACKNOWLEDGMENTS

This work was supported by the NSF under Grant No. DMR-8906003.

[1]G. A. Held, J. L. Jordan-Sweet, P. M. Horn, A. Mak, and R. J. Birgeneau, Phys. Rev. Lett. **59**, 2075 (1987).

[2]S. G. J. Mochrie, Phys. Rev. Lett. **59**, 304 (1987).

[3]Y. Cao and E. H. Conrad, Phys. Rev. Lett. **64**, 477 (1990).

[4]H. -N. Yang, T. -M. Lu, and G. -C. Wang, Phys. Rev. Lett. **63**, 1621 (1989).

[5]J. M. Kosterlitz and D. J. Thouless, J. Phys. C **6**, 1181 (1973); J. M. Kosterlitz, *ibid.* **7**, 1046 (1974).

[6](a) A. Trayanov, A. C. Levi, and E. Tosatti, Europhys. Lett. **8**, 657 (1989); (b) Surf. Sci. **233**, 184 (1990).

[7]U. Scheithauer, G. Meyer, and M. Henzler, Surf. Sci. **178**, 441 (1986).

[8]J. -K. Zuo, R. A. Harper, and G.-C. Wang, Appl. Phys. Lett. **51**, 250 (1987).
[9]T. -M. Lu and M. G. Lagally, Surf. Sci. **120**, 47 (1982).
[10]J. W. M. Frenken, F. Hussen, and J. F. van der Veen, Phys. Rev. Lett. **58**, 401 (1987).
[11]J. W. M. Frenken, J. F. van der Veen, R. N. Barnett, U. Landman, and C. L. Cleveland, Surf. Sci. **172**, 319 (1986).
[12]Y. S. Li, J. Quinn, F. Jona, and P. M. Marcus, Phys. Rev. B **40**, 8239 (1989).
[13]T. -M. Lu and M. G. Lagally, Surf. Sci. **99**, 695 (1982).
[14]J. M. Pimbley and T. -M. Lu, Surf. Sci. **139**, 360 (1984).
[15]K. Rommelse and Marcel den Nijs, Phys. Rev. Lett. **59**, 2578 (1987).
[16]J. W. M. Frenken and J. F. van der Veen, Phys. Rev. Lett. **54**, 134 (1985).
[17]J. D. Weeks, in *Ordering of Strongly Fluctuating Condensed Matter System,* edited by T. Riste (Plenum, New York, 1980), p. 293.
[18]H. van Beijeren and I. Nolden, in *Structures and Dynamics of Surface II,* edited by W. Schommers and P. Von Blanckenhage, Topics in Current Physics Vol. 43 (Springer-Verlag, Heidelberg, 1987), p. 259.
[19]S. T. Chui and J. D. Weeks, Phys. Rev. B **14**, 4978 (1976).
[20]H. van Beijeren, Phys. Rev. Lett. **38**, 993 (1973).
[21]R. W. Youngblood, J. D. Axe, and B. M. McCoy, Phys. Rev. B **21**, 5212 (1980); R. W. Youngblood and J. D. Axe, *ibid.* **23**, 232 (1981).
[22]J. Villain, D. R. Grempel, and J. Lapujoulade, J. Phys. F **15**, 809 (1985).
[23]W. Selke and A. M. Szpika, Z. Phys. B **62**, 381 (1986); W. Selke, J. Phys. C **20**, L455 (1987).
[24]B. Salanon, F. Fabre, J. Lapujoulade, and W. Selke, Phys. Rev. B **38**, 7385 (1988).
[25](a) J. M. Pimbley and T. -M. Lu, J. Vac. Sci. Technol. A **2**, 457 (1984); (b) J. Appl. Phys. **57**, 1121 (1985); (c) **57**, 4583 (1985); (d) **59**, 2493 (1986).
[26]C. S. Lent and P. I. Cohen, Surf. Sci. **139**, 121 (1984).
[27]P. Dutta and S. K. Sinha, Phys. Rev. Lett. **47**, 50 (1981).
[28]*Handbook of Mathematical Functions,* edited by M. Abramowitz and I. A. Stegun (Dover, New York, 1970).
[29]I. K. Robinson, E. H. Conrad, and D. S. Reed, J. Phys. (Paris) **51**, 103 (1990).
[30]V. Pontikis and V. Rosato, Surf. Sci. **162**, 150 (1985).